First-principles atomistic study of surfaces of Fe-rich Fe–Cr

2011 J. Phys.: Condens. Matter 23 265004

(http://iopscience.iop.org/0953-8984/23/26/265004)

J. Phys.: Condens. Matter **23** (2011) 265004 (8pp) doi:10.1088/0953-8984/23/26/265004

First-principles atomistic study of surfaces of Fe-rich Fe–Cr

M Ropo[1,2,3,9], K Kokko[3,4], E Airiskallio[3], M P J Punkkinen[3,5], S Hogmark[6], J Kollár[7,10], B Johansson[5,8] and L Vitos[5,7,8]

[1] Department of Information Technology, Åbo Akademi University, FIN-20500 Turku, Finland
[2] Graduate School of Materials Research, Turku, Finland
[3] Department of Physics and Astronomy, University of Turku, FIN-20014 Turku, Finland
[4] Turku University Centre for Materials and Surfaces (MatSurf), Turku, Finland
[5] Applied Materials Physics, Department of Materials Science and Engineering, Royal Institute of Technology, SE-10044 Stockholm, Sweden
[6] Department of Engineering Sciences, Uppsala University, SE-751 21 Uppsala, Box 534, Sweden
[7] Research Institute for Solid State Physics and Optics, PO Box 49, H-1525 Budapest, Hungary
[8] Division of Materials Theory, Department of Physics and Materials Science, Uppsala University, PO Box 516, SE-75120 Uppsala, Sweden

E-mail: matti.ropo@utu.fi

Received 2 December 2010, in final form 10 May 2011
Published 6 June 2011
Online at stacks.iop.org/JPhysCM/23/265004

Abstract
The surface properties of Fe-rich ferromagnetic Fe–Cr alloys are investigated using a first-principles quantum-mechanical method. In dilute alloys, the surfaces are dominated by Fe, whereas the Cr-containing surfaces become favorable when the bulk Cr concentration exceeds the limit of ∼10 atomic per cent. The abrupt change in the surface behavior is the consequence of complex competing magneto-chemical interactions between the alloying atoms. Considering the quantities of various features: equilibrium surface profiles, chemical potentials, segregation energies, surface energies, magnetic moments, mixing energies and pair interactions, within a wider range of bulk and surface concentrations enables us to build a comprehensive picture of the physics of Fe–Cr surfaces. Using the present achievements many previously controversial results can now be merged into a consistent model of Fe-rich Fe–Cr alloys.

(Some figures in this article are in colour only in the electronic version)

1. Introduction

Iron-rich Fe–Cr alloys are the basic building blocks of ferritic stainless steels. The excellent corrosion resistance combined with good mechanical properties places these alloys among the most important engineering materials. Their corrosion rate decreases drastically within a narrow concentration interval (9–13 wt% Cr) [1–3], making the transition from iron-type to non-corrosive behavior quite abrupt. During oxidation, first a monolayer of oxide is formed instantly on the clean alloy surface exposed to an oxidizing environment. The type of the initial oxide layer depends on the oxygen pressure, temperature and the actual alloy compositions within the first few surface layers. The high surface density of the chemically less active atoms may also initiate the internal oxidation of the active alloy components. Focusing on the surface phenomena, further oxidation assumes transport of metal and oxygen ions through the initially formed oxide film. The ion transport is controlled by diffusion, which in turn is determined by the defect structure of the oxide layer. The high mobility of Fe in Fe oxides, especially in FeO, which is the dominant oxide component on pure iron above 570 °C, explains the corrosive nature of Fe. The passivity in Fe–Cr, on the other hand, is attributed to a stable Cr-rich oxide scale. Above the critical concentration a pure chromia layer is formed which effectively blocks the ion diffusion across the oxide scale.

[9] Present address: Fritz-Haber-Institut der Max-Planck-Gesellschaft, D-14195 Berlin, Germany.
[10] Deceased.

Describing the oxide layer growth and ultimately the passivity of stainless steels is an enormous task as it requires knowledge of the thermodynamic and kinetic properties of the oxide as well as oxide–metal and oxide–gas interfaces under oxidizing conditions. Often the kinetics of the oxidation process is so slow that the real thermodynamic equilibrium is never reached during the active lifetime of the alloy product. Today a great deal of information is available about the properties of the oxide scale on Fe–Cr, but the initial stage of the oxidation is still unclear. This is due to the experimental difficulties connected to the timescale of the initial oxidation of clean alloy surfaces. A large number of models were put forward for the kinetics of the thin layer oxidation and oxide scale formation [2]. Most of these theories, however, left in the shadow the active role of the metallic substrate in the oxidation process, simplifying it to a cation and electron reservoir. This might be a justified approximation after a monolayer or a few layers of oxide are built up. Nevertheless, the atomic level behavior of the metallic Fe–Cr surfaces is indispensable for understanding the oxygen chemisorption and the initial thin layer oxide formation on this class of materials.

Numerous former first-principles calculations focused on the properties of the Fe-rich Fe–Cr surfaces [4–7]. However, due to the involved approximations and constraints, most of these studies failed to reproduce the experimentally observed Cr enrichment on the alloy surface [8]. Later, using the exact muffin-tin orbital method [9–12] in combination with the generalized gradient approximation [13], it was demonstrated that the Fe–Cr surfaces exhibit a compositional threshold behavior [14]. In particular, we showed that about 9 at.% chromium in Fe–Cr induces a sharp transition from Cr-free surfaces to Cr-containing surfaces. This surprising surface behavior was found to be a consequence of the complex bulk and surface magnetic interactions characteristic to the Fe–Cr system. The predicted surface chemical threshold has recently been confirmed by an independent theoretical study by Kiejna and Wachowicz [15].

In the present paper, further details about our theoretical study of the surface and magnetic properties of the iron-rich Fe–Cr alloys are presented. In section 2 we briefly review the computational tools and in section 3 we present the theoretical predictions for the Fe–Cr surfaces. A comprehensive analysis of the bulk and surface magnetic structures as well as the Cr–Cr interactions is given. In addition to the equilibrium surface concentration profiles, the non-equilibrium states are also discussed emphasizing the role of the effective chemical potential as being a driving force for Cr diffusion toward the free surfaces.

2. Details of calculations

The first-principles quantum-mechanical calculations were performed in the framework of density functional theory [16]. The Kohn–Sham equations [17] were solved using the exact muffin-tin orbital method (EMTO) [9–12] and for the total energy the full charge density formalism was employed [10, 18]. Substitutional disorder was treated within the coherent potential approximation (CPA) [19, 20, 11]. The one electron equations were solved using the scalar-relativistic and soft-core approximations. The Green's function was calculated for 32 complex energy points distributed exponentially on a semi-circular contour and the basis set included s, p, d, and f orbitals. The exchange–correlation potential was treated using the generalized gradient approximation by Perdew *et al* [13] Theoretical equilibrium lattice constants (a) were used throughout the calculations.

The thermodynamically stable surface of the $Fe_{1-c}Cr_c$ alloys was modeled by periodic slab geometry with eight (100) atomic layers plus four empty layers representing the vacuum region. All atomic positions were kept fixed to the ideal body-centered cubic (bcc) positions. It is well known that the free surfaces of pure metals and alloys adopt different crystal structures from those of ideally truncated bulk crystals. Upon layer relaxation only rigid inward or outward displacement of the atomic layers occurs, while in the case of reconstruction, the displacement of atoms may alter the two-dimensional symmetry of the surface. In the case of close-packed transition metal surfaces reconstructions are less common, but layer (or multi-layer) relaxation has often been observed. Recent first-principles studies [21] demonstrate that the bcc (001) surfaces of Fe and Cr show only minor inward relaxations. The unusually small surface relaxation (compared to the corresponding 4d [22] or 5d [23, 24] metals) is due to the enhanced surface magnetism, which gives a positive contribution to the surface pressure. On these grounds, we expect that in Fe-rich Fe–Cr alloys the surface structure indeed remains close to the ideal bulk geometry.

The chemical composition of the first surface layer was optimized whereas the concentration of the other six layers were fixed to the bulk concentration c. In real materials the surface effects may alter the ideal bulk-like chemistry within several surface layers. The Fe–Cr binary system forms a regular solid solution with a large miscibility gap. Phase separation takes place via nucleation and growth and spinodal decomposition. Performing a multi-layer chemical relaxation would assume that at low temperature one can properly account for the above effects in the bulk part of the slab. Unfortunately, this is beyond the scope of our approach. On the other hand, at elevated temperature the phase separation becomes less important and a random solid-solution model adopted in the present work is supposed to properly describe the bulk Fe–Cr system. According to the Fe–Cr phase diagram, at 1000 K (500 K) the solubility limit is 25% (10%) Cr. The present approach is expected to work reasonably well for this composition and temperature interval.

In magnetic systems, surface magnetism reduces the surface energy of open surfaces to the extent that the usual anisotropy of the surface energy is reversed [25–27]. In particular, the magnetic contribution to the surface energy of the (100) facet of pure Cr (Fe) is about −50% (−41%) compared to −2% (−16%) obtained for the close-packed (110) facet [25]. Accordingly, the surface calculations were performed for the (100) crystal facet of the B2 lattice and for the (100) crystal facet of the bcc lattice, which are the most stable surfaces for pure Cr and for Fe-rich Fe–Cr alloys, respectively.

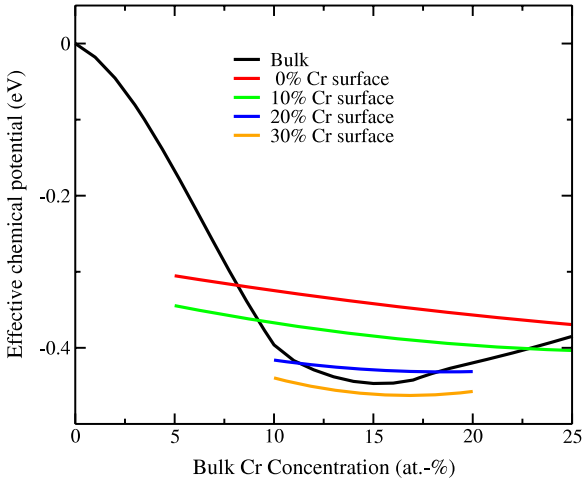

Figure 1. Effective bulk (black curved line) and surface chemical potentials (in electronvolts) of ferromagnetic $Fe_{1-c}Cr_c$ alloys as a function of bulk Cr concentration (at.%) at $T = 0$ K. The surface effective chemical potentials are shown by shorter lines, from top to bottom: 0 at.% (red), 10 at.% (green), 20 at.% (blue) and 30 at.% (yellow) Cr in the surface layer. All curves are plotted relative to the bulk effective chemical potential for the dilute alloy, which is −6036.006 eV/atom according to our calculations.

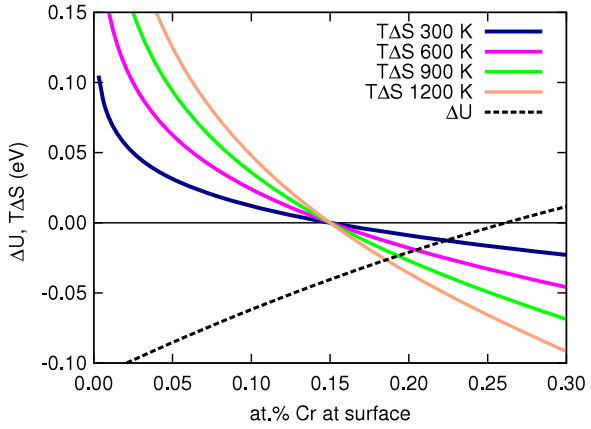

Figure 2. The variations in the internal energy (ΔU) and the entropy part ($T\Delta S$) of the $Fe_{0.85}Cr_{0.15}$ alloy for an atomic pair bulk surface Cr ↔ Fe exchange. The intersection points of the ΔU and $T\Delta S$ curves give the equilibrium Cr concentration of the surface at a given temperature T.

The surface concentration of Cr (c^s) of the $Fe_{1-c}Cr_c$ alloy was determined by minimizing the grand potential of the surface [28, 29]:

$$\Omega^S = U - TS + \Delta\mu^b n_s(c^s - c), \tag{1}$$

where U, T, S, $\Delta\mu^b \equiv \mu_{Fe} - \mu_{Cr}$, and n_s are the internal energy, temperature, entropy, effective chemical potential in the bulk, and the number of atoms in the surface layer of the slab, respectively. In equation (1) all thermodynamic functions depend on the bulk and surface concentrations. Considering only the configurational part of the entropy yields

$$\Omega^S(c, c^s) = U^S(c, c^s) + 2k_BT[c^s \ln c^s + (1 - c^s)\ln(1 - c^s)] + 2\{\Delta\mu_0^b(c) - k_BT[\ln c - \ln(1 - c)]\}(c^s - c), \tag{2}$$

where k_B is the Boltzmann constant, $\Delta\mu_0^b$ is the zero-temperature effective chemical potential in the bulk, and the internal energy $U^S(c, c^s)$ is obtained from *ab initio* surface slab calculations. The second factor in equation (2) results from the two surfaces of the slab.

3. Results and discussion

3.1. Chemical composition of the surfaces

To shed light on the atomic origin of the chemical threshold behavior of Fe–Cr surfaces [14], we first investigate the effective chemical potentials (ECPs) of the bulk ($\Delta\mu^b$) and the (100) surface ($\Delta\mu^s$). In figure 1, the bulk and surface ECP are plotted as a function of bulk Cr concentration. Data are shown for surfaces containing 0, 10, 20, and 30 at.% Cr. Comparing these curves one can easily construct a clear picture of the driving forces behind the peculiar trend of the surface chemistry of Fe–Cr alloys. At low Cr bulk concentrations ($c < 0.08$), the ECP in bulk is above the ECP at the pure Fe surface. As a consequence, for these alloys the Fe terminated surface is more favorable than the Cr-containing surface. For Cr atoms there is a large chemical driving force from the surface toward the bulk. Notice that this finding is in perfect agreement with previous *ab initio* calculations [5]. However, near 8 at.% Cr in the bulk alloy the bulk ECP drops below the surface ECP, which marks the beginning of the transition from pure Fe terminated surfaces to Cr-containing surfaces. Our finding of the outburst of bulk Cr to the surface at about 8–9 at.% Cr in the bulk agrees well with the theoretical prediction based on the Ising model [30].

At a given temperature T the equilibrium surface concentration of Cr can be estimated also by considering an atomic exchange process where a Cr atom in the bulk and an Fe atom at the surface are interchanged. While during this exchange process the temperature, volume and number of atoms of the system are held constant the equilibrium state can be found by minimizing the Helmholtz free energy, $F = U - TS$, of the system. Therefore, one obtains an estimate for the equilibrium surface concentration of the considered alloy by posing the requirement $dU(c, c^s) = TdS(c, c^s)$, provided that c^s is within the limits $0 < c^s < 1$. To illustrate the described method we show in figure 2 the variations, per atomic pair, of the entropy part (TS) and the internal energy of $Fe_{0.85}Cr_{0.15}$, as a function of the Cr concentration at the surface layer. The variation of the internal energy is estimated as $\Delta U = \Delta\mu^b - \Delta\mu^s$, where $\Delta\mu = \mu_{Fe} - \mu_{Cr}$ and the superscripts b and s refer to the bulk and surface subsystems, respectively. The variations $T\Delta S$ form a set of curves corresponding to different temperatures with the obvious intersection point at $c^s = c$. The intersection points of ΔU and $T\Delta S$ curves give the equilibrium surface concentrations at corresponding temperatures. For the $Fe_{0.85}Cr_{0.15}$ alloy we get the equilibrium surface concentrations starting from about 25 at.% at 0 K down to 18 at.% at 1200 K. For alloys of different bulk

Table 1. Theoretical equilibrium Cr concentration in the (100) surface layer of ferromagnetic $Fe_{1-c}Cr_c$ alloys. Results are listed for $c = 0.001$, 0.05, 0.10, 0.15, and 0.20 for temperatures 300 and 700 K.

Bulk Cr concentration	T (K)	Surface Cr concentration
0.001	300	0.00
0.05	300	0.00
0.10	300	0.14
0.15	300	0.22
0.20	300	0.17
0.001	700	0.00
0.05	700	0.01
0.10	700	0.13
0.15	700	0.20
0.20	700	0.18

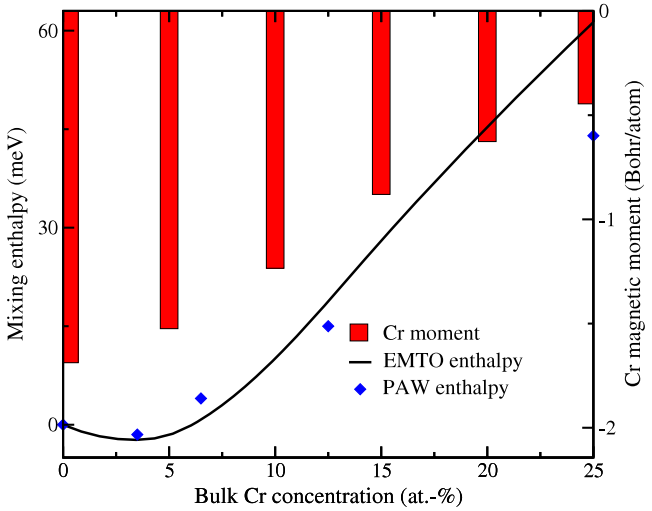

Figure 3. Left axis: the mixing enthalpy of Fe–Cr as a function of the bulk Cr concentration. Diamonds are projector augmented wave (PAW) enthalpy results by Olsson *et al* [34]. Right axis: Cr magnetic moments in ferromagnetic Fe–Cr alloys.

concentration the above picture would change simply as follows: the set of entropy curves ($T\Delta S$) would shift left or right with decreasing or increasing Cr concentration in bulk, respectively. The internal energy curve (ΔU), instead, will shift upwards whenever the bulk Cr concentration deviates from $c = 0.15$ value. This is justifiable according to figure 1, that is $c = 0.15$ corresponds to the minimum point of the bulk ECP curve, whereas the surface effective potential curves have approximately the same slope irrespective of the bulk concentration.

Table 1 lists our theoretical results for the equilibrium Cr concentrations at the (100) surface for five bulk compositions and two temperatures. The highest Cr content at the surface is obtained for the $Fe_{0.85}Cr_{0.15}$ alloy. In this case the surface Cr concentration at 0 K temperature is about 1.7 times the bulk value. The corresponding experimental results show a large variation, but on average the measured surface Cr content is typically 1.5–3 times the bulk value [31–33]. Our calculations for the atomic layer just below the surface layer show that Fe enrichment is expected in the second layer at the threshold value of the bulk composition. The ECP $\Delta\mu$ for the second layer is about 0.3 eV lower than the bulk value for the 10 at.% Cr in bulk. This is of the same order of magnitude as the difference between the surface and bulk ECPs at the dilute alloy limit (figure 1).

From figure 1, we can see that the transition from Fe terminated surfaces to Cr-containing surfaces is to a large degree due to the change of the bulk ECP as the changes in the surface ECPs are small within the investigated concentration region. Therefore, the transition in surface chemistry can be addressed to originate mainly from the bulk. Of course, the question could be formulated also as: why is the surface chemical potential so different from its bulk counterpart? In the following we will give further support for the bulk-induced scenario. The mixing enthalpy of bulk $Fe_{1-c}Cr_c$ is

$$\Delta H^{\mathrm{b}}(c) = E^{\mathrm{b}}(c) - cE^{\mathrm{b}}(\mathrm{Cr}) - (1-c)E^{\mathrm{b}}(\mathrm{Fe}), \qquad (3)$$

where $E^{\mathrm{b}}(c)$, $E^{\mathrm{b}}(\mathrm{Cr})$ and $E^{\mathrm{b}}(\mathrm{Fe})$ are the equilibrium energies for ferromagnetic bcc alloy, antiferromagnetic Cr and ferromagnetic Fe, respectively. The present theoretical $\Delta H^{\mathrm{b}}(c)$ is compared with full-potential results [34] in figure 3. Both theoretical enthalpies are negative at small Cr concentrations ($\lesssim$6–7 at.%) and they change their curvature at around 15 at.% Cr. It is important to point out that the mixing enthalpy from figure 3 corresponds to the ferromagnetic phase. Paramagnetic Fe–Cr forms a regular solid solution with positive mixing enthalpy for the entire concentration range [35].

To connect the mixing enthalpy to the ECP, we take the first order concentration derivative of $\Delta H^{\mathrm{b}}(c)$, namely

$$\frac{\mathrm{d}\Delta H^{\mathrm{b}}(c)}{\mathrm{d}c} = \frac{\mathrm{d}E^{\mathrm{b}}(c)}{\mathrm{d}c} - E^{\mathrm{b}}(\mathrm{Cr}) + E^{\mathrm{b}}(\mathrm{Fe}) \approx -\Delta\mu_0^{\mathrm{b}}(c) + C, \qquad (4)$$

where C is a constant and the small volume effects in the second part of the equation have been neglected. According to this expression, the negative of the bulk ECP exhibits the same concentration dependence as the derivative of the mixing enthalpy. Considering the second order derivative of the mixing enthalpy, we obtain

$$\frac{\mathrm{d}^2\Delta H^{\mathrm{b}}(c)}{\mathrm{d}c^2} \approx -\frac{\mathrm{d}\Delta\mu_0^{\mathrm{b}}(c)}{\mathrm{d}c}, \qquad (5)$$

that is the curvature of $\Delta H^{\mathrm{b}}(c)$ is the negative of the slope of bulk ECP. Therefore, the large positive curvature of the ferromagnetic $\Delta H^{\mathrm{b}}(c)$ below $c \approx 0.15$ is reflected by the negative slope of $\Delta\mu_0^{\mathrm{b}}(c)$. In other words, the steep decrease in bulk chemical potential at small Cr concentrations (figure 1) and consequently the peculiar transition in surface chemistry can be traced to the anomalous mixing between Fe and Cr atoms in the bcc lattice.

The anomalous mixing between Fe and Cr can be understood by investigating the bulk electronic structure of ferromagnetic Fe–Cr [34]. Neglecting the electrostatic and exchange–correlation contributions, the mixing enthalpy of a

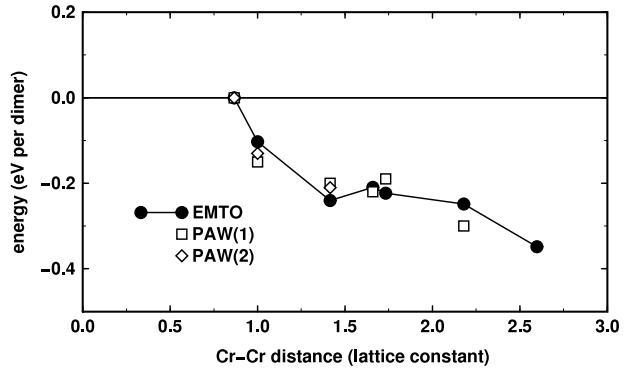

Figure 4. Calculated total energy (in electronvolts) for a ferromagnetic Cr–Cr dimer in bcc Fe as a function of Cr–Cr separation (in units of bcc lattice constant). The present result (EMTO) is compared to other theoretical results calculated using the PAW method. To enable comparison between different data, the energies have been plotted relative to the energy of the nearest-neighbor configuration. PAW(1) [39] refers to data obtained for a sufficiently large number of k-points for absolute-energy convergence, but using a relatively small (24 atoms) supercell. PAW(2) [40] refers to data obtained for a $3 \times 3 \times 3$ bcc supercell (54 atoms), using only 125 k-points in the Brillouin zone and taking into account the local relaxation around the Cr–Cr dimers.

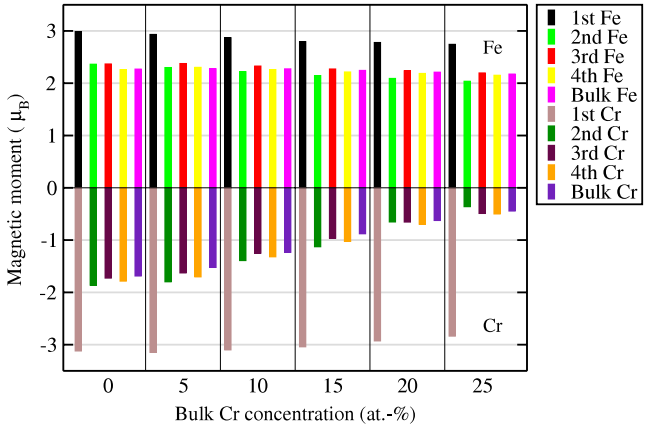

Figure 5. The magnetic moments (in units of Bohr magneton μ_B) of Fe and Cr atoms in different surface layers for a homogeneous slab and bulk as a function of Cr bulk concentration.

binary alloy can be approximated by the band energy term $\Delta H^{\mathrm{b}}(c) \approx \Delta E^{\mathrm{b}}_{\mathrm{one}}(c) = E^{\mathrm{b}}_{\mathrm{one}}(c) - cE^{\mathrm{b}}_{\mathrm{one}}(\mathrm{Cr}) - (1-c)E^{\mathrm{b}}_{\mathrm{one}}(\mathrm{Fe})$. A small amount of Cr addition to Fe shifts the antibonding bcc peak in the majority spin channel toward lower energies (see figure 4, [34]) and as a consequence $E^{\mathrm{b}}_{\mathrm{one}}(c)$ is lowered relative to the average band energy, yielding $\Delta E^{\mathrm{b}}_{\mathrm{one}}(c) < 0$. With increasing Cr concentration, the majority spin channel is gradually emptied and the density of states at the Fermi level increases, which results in positive $\Delta E^{\mathrm{b}}_{\mathrm{one}}(c)$. The physical origin of the above trend can be related to the Fe–Fe, Fe–Cr, and Cr–Cr magneto-chemical interactions.

3.2. Interplay of magnetic moments

The limited solubility of chromium in iron is linked to complex magnetic interactions between antiferromagnetic chromium and ferromagnetic iron [36, 35]. In Fe-rich Fe–Cr alloys, Cr moments couple anti-parallel with the Fe matrix and therefore Cr atoms are necessarily coupled parallel to each other. It has been shown that this magnetic frustration has a key role on the miscibility of the Fe–Cr alloys [36]. Here we illustrate this effect by considering the interaction energy of a ferromagnetic Cr–Cr pair in a bulk Fe matrix. To this end, we considered a supercell containing 52 Fe atoms and 2 Cr atoms, and computed the total energy difference as a function of Cr–Cr dimer distance. In figure 4, we compare our Cr–Cr interactions with those obtained using the Vienna *ab initio* simulation package (VASP) in combination with the PAW method [37, 38].

For the interaction energy of Cr–Cr dimer at third-, second- and first-neighbor configurations we obtained 8 meV, 145 meV and 248 meV, respectively, where the reference level was fixed to the average energy calculated using the last four points in figure 4. Note that the repulsive interaction energy increases dramatically for the first and second neighbors (14 sites). Since the interaction energy between the Cr atoms sitting on distant bcc sites is small, this has only a small effect on the stability of dilute Fe–Cr alloys. However, as the Cr concentration increases in the alloy, the second- and first-nearest-neighbor Cr pairs appear more and more frequently and the associated large repulsive interactions decrease the average cohesion within the system and push the mixing enthalpy curve upwards. The system lowers these energetically unfavorable magnetic interactions by the following main mechanisms: the average moment of Cr decreases, Cr-rich clusters are formed and finally Cr atoms are pushed toward the alloy surface. In the following we illustrate the first mechanism by monitoring the surface and bulk magnetic moments as a function of bulk composition. The second mechanism has been studied by Klaver *et al* [39] and the third one is demonstrated in figure 1.

In figure 5 the magnetic moments in the first four surface atomic layers and in the bulk are presented. Data are shown starting from the impurity level up to 25 at.% Cr in the bulk. The Fe moments in the surface layers as well as in the bulk show a small decrease with increasing Cr concentration. In the topmost surface layer, the Cr moment (1st Cr) behaves similarly as Fe. The subsurface and bulk Cr moments, on the other hand, exhibit a strong composition dependence. These moments decrease from $\sim$1.7 μ_B to $\sim$0.4 μ_B as the Cr concentration increases from 0 to 25 at.%. This decrease of the Cr moments can be related to the increase of the unfavorable Cr interactions with increasing Cr concentration in the alloy.

In line with our results the enhanced moments at the surface layer have been obtained also for mixed Cr overlayers on Fe(100) [41, 42]. Moreover, our results for the Cr moments in different surface layers in dilute Fe–Cr alloy are in good agreement with those of Kiejna and Wachowicz [15]. When increasing the Cr concentration in bulk we obtained a decreasing trend (a slight decrease) for the Cr (Fe) moments in the bulk alloy. This result compares well with other theoretical

results [39, 43]. Besides these theoretical investigations the element-resolved magnetic measurements show trends similar to our data [44].

Interestingly, the Cr–Cr interactions in the bulk and at the (100) surface show different behavior leading to the different immiscibility thresholds in the bulk and at the surface as well. Mixing of Cr in Fe is easier at the surface than in the bulk. This conclusion can be drawn on the basis of figure 1. The ECP at the surface has a negative slope up to the largest concentrations considered (30 at.%) whereas the slope of the bulk ECP is changed from negative to positive much earlier, at about 15 at.%. According to equation (4) the slope of the ECP and the curvature of the mixing enthalpy are related in a way that the negative slope of the ECP corresponds to the positive curvature of the mixing enthalpy, i.e. the case of miscible systems. The increased miscibility at the surface can be understood by geometric considerations. When going on from the bulk to the surface atomic layer, the drop of the dimensions of the system from three to two changes the relation between the Cr concentration and the average distance between the nearest-neighbor Cr atoms. For instance, the average nearest-neighbor distance of the Cr atoms in the (100) surface containing 25 at.% Cr is $2a$, whereas in the bulk bcc the same average nearest-neighbor distance $2a$ is reached much earlier, already at the level of 6.25 at.% Cr. As mentioned in section 3.1 bulk alloys of 6.25 at.% Cr are barely stable. Therefore, a complete parallelism between bulk and surface interactions explains the stability of surfaces at least up to 25 at.% Cr. However, the actual energy cost of the interaction scales with the number of atoms in the coordination shell which is always larger in the bulk: 6(12) for bulk and 4(4) for the surface when the average nearest-neighbor Cr–Cr distance is $2a$ ($\sqrt{2}a$). This effect pushes the upper bound of miscibility at the surface to still higher Cr concentrations. For instance, if the average Cr–Cr nearest-neighbor distance is $\sqrt{2}a$ the energy cost per Cr atom at the surface (50 at.% alloying) is $\frac{1}{2} \times 4 \times 8$ meV $= 16$ meV and in the bulk (25 at.% alloying) it is much higher $\frac{1}{2} \times 12 \times 8$ meV $= 48$ meV. Here the Cr–Cr dimer energy is taken to be the third-neighbor configuration energy 8 meV.

3.3. Energetics of the surfaces

After discussing the properties of the pure surfaces we enter the energetics of the surfaces and its relation to the corrosion resistance of Fe–Cr alloys. In the case of the passive oxide layer being destroyed, e.g. by mechanical scratching, a new clean metal surface is created and depending on the bulk concentration a surface containing Cr or a pure Fe surface is energetically the most favorable outcome. According to figure 1 in cases where the Cr content in bulk is between 9 and 19 at.%, due to the chemical potential imbalance, the bulk terminated surfaces tend to enrich with Cr, whereas for other alloys the tendency is to Cr-diluted surfaces. Obviously this has important consequences for the initial oxidation of surfaces. The type of the new surface determines to a large degree which kind of initial oxide layer is formed on the surface and consequently it is directly related to the corrosion resistance of the material at later stages. One should also note that a clear peak in the measured Cr/Fe atomic ratio is observed at the polished surface of the Fe–15Cr alloy [45]. However, it would be also interesting to see how the Cr/Fe ratio depends on the bulk composition of the alloy.

Table 2. Surface segregation energies of Cr (in electronvolts). c^s and c are the concentrations of Cr at the surface and in the bulk, respectively.

	c			
c^s	0.05	0.10	0.15	0.20
0.00	0.14	−0.07	−0.11	−0.06
0.10	0.17	−0.03	−0.06	−0.03
0.20		0.02	−0.02	0.01
0.30		0.04	0.01	0.01

The surface segregation energy of Cr in $Fe_{1-c}Cr_c$, defined as

$$E_{\text{segr}} = \frac{\mathrm{d}U}{\mathrm{d}c^s}, \tag{6}$$

has been considered as a controversial phenomenon. Different experiments have shown opposite results. Suzuki *et al* [33] investigated $Fe_{77}Cr_{13}$ and $Fe_{75}Cr_{25}$ using angle-resolved x-ray photoelectron spectroscopy and observed Cr enrichment at the surface at 973 K. On the other hand, Davies *et al* using scanning tunneling microscopy [46] and Venus and Heinrich using angle-resolved Auger electron spectroscopy [47] observed that Cr migrated toward bulk when Cr had been deposited on Fe. This was considered as a contradiction and several theoretical attempts were suggested to solve this controversy [6, 4, 5, 7]. Our surface segregation energies of Cr in table 2 can be compared with other theoretical segregation energies. Ponomareva *et al* [7] used both EMTO and PAW methods. With EMTO they calculated the diluted alloy limit and obtained 1.80–1.85 eV for the surface segregation energy of Cr. In table 2 the closest data to the dilute limit of the alloy are found in the ($c = 0.05$, $c^s = 0.00$) case which corresponds to the segregation energy of 0.14 eV. Our estimate for the diluted limit is 0.23 eV. The PAW results are for supercells corresponding to bulk concentrations below or at the border of the Cr surface segregation threshold and the surface concentrations above 10 at.%. Their segregation energies for unrelaxed lattices are from −0.01 to 0.14 eV. These results can be compared to our data in table 2 for the concentrations ($c = 0.05$, $c^s = 0.10$ and $c = 0.10$, $c^s = 0.10$–0.20) which correspond to segregation energies from −0.03 to 0.17 eV. Ruban *et al* [6] have calculated the dilute limit Cr surface segregation energies by the Green's function linear muffin-tin orbitals method in conjunction with the coherent potential and atomic sphere approximations including a multipole correction to the electrostatic potential and energy. Their result is about 0.2 eV, which compares well with our diluted alloy limit 0.23 eV. According to our results, shown in table 2, there is no real controversy in the experimental results of surface segregation of Cr in $Fe_{1-c}Cr_c$ alloys. As shown in table 2, the surface segregation energy of Cr is negative within a restricted concentration window, from about 10 to 20 at.% Cr in bulk

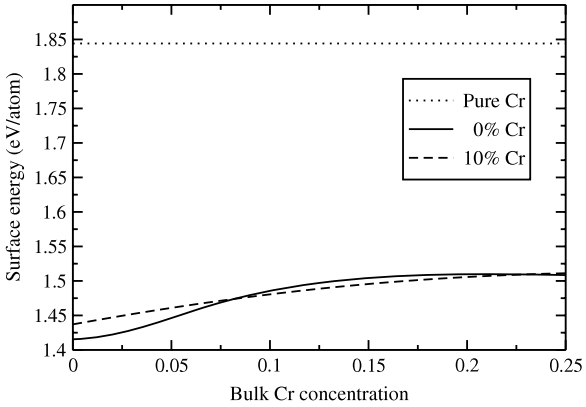

Figure 6. Surface energy of different alloy surfaces. The surface energy of Cr has been given as a comparison.

Fe–Cr and the surface concentration of Cr being less than 10–20 at.%. Therefore, it is natural that the experiments done for Cr deposition on Fe show the driving force of Cr into the bulk whereas the experiments done for alloys having about 10–20 at.% Cr in bulk show Cr enrichment at the surface.

The understanding of the behavior of the surface energy of Fe–Cr plays a useful role when one tries to understand the self-healing properties of stainless steels. In figure 6 the surface energies for two different surface concentrations (0 and 10 at.% Cr at the surface layer) and as a reference the surface energy of pure Cr metal are presented. For low Cr alloys the pure Fe surface has the lowest surface energy, but at around 8 at.% Cr the order is reversed and the Cr-containing surfaces become favorable. This reversing of the surface energies correlates well with the observed decrease of the corrosion rate in stainless steels [1].

4. Conclusion

Using state of the art density functional calculations we have investigated the surface and bulk properties of iron-rich Fe–Cr alloys. The computations were made using the exact muffin-tin orbital method combined with the generalized gradient approximation and the coherent potential approximation. We have shown how the changes in energetic and magnetic properties in the bulk and the relative stability of surface properties play an important role in the threshold behavior of the surface concentration in the iron-rich Fe–Cr alloys. The results of surface segregation experiments of Fe–Cr alloys, generally considered controversial, find their natural explanation when the energetics of Fe–Cr surfaces are studied systematically within larger concentration regions. The discovered reversals of surface energies and chemical potentials are in line with the sharp decrease of the experimental corrosion rate of the ferritic steels appearing at 9–13 wt% Cr. The onset of corrosion resistance in ferritic steels agrees well with the theoretical prediction of the outburst of Cr from the bulk to the surface at 8–9 at.% Cr. The threshold behavior of the surface composition can be related to the frustration in magnetic interactions in bulk Fe–Cr.

Acknowledgments

The computer resources of the Finnish IT Centre for Science (CSC) and Mgrid project are acknowledged. Part of this work was supported by the Swedish Research Council, the Swedish Steel Producers' Association, the Göran Gustafsson Foundation, the Hungarian Scientific Research Fund (research project OTKA 84078), and the Academy of Finland (Grant No. 116317).

References

[1] Wranglén G 1985 *An Introduction to Corrosion and Protection of Metals* (New York: Chapman and Hall)
[2] Khanna A S 2002 *Introduction to High Temperature Oxidation and Corrosion* (Metals Park, OH: ASM International)
[3] Ryan M P, Williams D E, Chater R J, Hutton B M and McPhail D S 2002 *Nature* **415** 770
[4] Nonas B, Wildberger K, Zeller R and Dederichs P H 1998 *Phys. Rev. Lett.* **80** 4574
[5] Geng W T 2003 *Phys. Rev.* B **68** 233402
[6] Ruban A V, Skriver H L and Nørskov J K 1999 *Phys. Rev.* B **59** 15990
[7] Ponomareva A V, Isaev E I, Skorodumova N V, Vekilov Y K and Abrikosov I A 2007 *Phys. Rev.* B **75** 245406
[8] Dowben P A, Grunze M and Wright D 1983 *Surf. Sci.* **134** L524
[9] Andersen O K, Jepsen O and Krier G 1994 Exact muffin-tin orbital theory *Lectures on Methods of Electronic Structure Calculations* ed V Kumar, O K Andersen and A Mookerjee (Singapore: World Scientific) pp 63–124
[10] Vitos L 2001 *Phys. Rev.* B **64** 014107
[11] Vitos L, Abrikosov I A and Johansson B 2001 *Phys. Rev. Lett.* **87** 156401
[12] Vitos L 2007 Computational quantum mechanics for materials engineers: the EMTO method and applications *Engineering Materials and Processes* (London: Springer)
[13] Perdew J P, Burke K and Ernzerhof M 1996 *Phys. Rev. Lett.* **77** 3865
[14] Ropo M, Kokko K, Punkkinen M P J, Hogmark S, Kollár J, Johansson B and Vitos L 2007 *Phys. Rev.* B **76** 220401(R)
[15] Kiejna A and Wachowicz E 2008 *Phys. Rev.* B **78** 113403
[16] Hohenberg P and Kohn W 1964 *Phys. Rev.* **136** B864–71
[17] Kohn W and Sham L J 1965 *Phys. Rev.* **140** A1133
[18] Kollár J, Vitos L and Skiver H L 2000 From ASA towards the full potential *Electronic Structure and Physical Properties of Solids: The Uses of the LMTO Method* (*Lecture Notes in Physics*) ed H Dreysse (Berlin: Springer) pp 85–113
[19] Soven P 1967 *Phys. Rev.* **156** 809
[20] Györffy B L 1972 *Phys. Rev.* B **5** 2382
[21] Punkkinen M P J, Kwon S K, Kollár J, Johansson B and Vitos L 2011 *Phys. Rev. Lett.* **106** 057202
[22] Kwon S K, Nabi Z, Kádas K, Kollár J, Vitos L, Johansson B and Ahuja R 2005 *Phys. Rev.* B **72** 235423
[23] Zólyomi V, Kollár J and Vitos L 2008 *Phys. Rev.* B **78** 195414
[24] Zólyomi V, Vitos L, Kwon S K and Kollár J 2009 *J. Phys.: Condens. Matter* **21** 095007
[25] Aldén M, Skriver H L, Mirbt S and Johansson B 1994 *Surf. Sci.* **315** 157
[26] Vitos L, Ruban A V, Skriver H L and Kollár J 1998 *Surf. Sci.* **411** 186
[27] Aldén M, Skriver H L, Mirbt S and Johansson B 1992 *Phys. Rev. Lett.* **69** 2296
[28] Ropo M, Kokko K, Vitos L, Kollár J and Johansson B 2006 *Surf. Sci.* **600** 904–13

[29] Ropo M 2006 *Phys. Rev.* B **74** 195401
[30] Ackland G J 2009 *Phys. Rev.* B **79** 094202
[31] Leygraf C, Hultquist G, Ekelund S and Eriksson J C 1974 *Surf. Sci.* **46** 157
[32] Lince J R, Didziulis S V, Shuh D K, Durbin T D and Yarmoff J A 1992 *Surf. Sci.* **277** 43
[33] Suzuki S, Kosaka T, Inoue H, Isshiki M and Waseda Y 1996 *Appl. Surf. Sci.* **103** 495
[34] Olsson P, Abrikosov I A and Wallenius J 2006 *Phys. Rev.* B **73** 104416
[35] Olsson P, Abrikosov I A, Vitos L and Wallenius J 2003 *J. Nucl. Mater.* **321** 84
[36] Ackland G J 2006 *Phys. Rev. Lett.* **97** 015502
[37] Kresse G and Hafner J 1993 *Phys. Rev.* B **47** R558
[38] Kresse G and Hafner J 1994 *Phys. Rev.* B **49** 14251
[39] Klaver T P, Drautz R and Finnis M W 2006 *Phys. Rev.* B **74** 094435
[40] Olsson P, Domain C and Wallenius J 2007 *Phys. Rev.* B **75** 014110
[41] Herper H C, Hoffmann E and Entel P 2002 *J. Magn. Magn. Mater.* **240** 401
[42] Herper H C, Hoffmann E and Entel P 2002 *Phase Transit.* **75** 185
[43] Ruban A V, Korzhavyi P A and Johansson B 2008 *Phys. Rev.* B **77** 094436
[44] Kortright J B, Kim S-K and Ohldag H 2000 *Phys. Rev.* B **61** 64
[45] Park E, Hüning B and Spiegel M 2005 *Appl. Surf. Sci.* **249** 127
[46] Davies A, Stroscio J A, Pierce D T and Celotta R J 1996 *Phys. Rev. Lett.* **76** 4175
[47] Venus D and Heinrich B 1996 *Phys. Rev.* B **53** R1733